than the value predicted by the K^* dominance model, which also accounts^{4,8} for the magnitude of the vector form factor in K_{e3}^+ .

We remark finally that a weakly interacting intermediate vector boson (W) may also mediate the decay $K \rightarrow e\nu\gamma$. The form factor obtained using the W as an intermediate state is12

$$f(p^{K} \cdot p^{\gamma}) = \frac{(bg_{W}^{2}/M_{W}^{2})[2 - \mu_{W} - Q_{W}(p^{\gamma} \cdot p^{K}/2M_{W}^{2})]}{M_{W}^{2} - M_{K}^{2} + 2p^{K} \cdot p^{\gamma}}.$$
 (12)

Reference 12 obtains the value of the coupling constant b from the experimental value of the kaon lifetime, and the value of g_{W^2}/M_{W^2} from the β decay coupling constant. The branching ratio $\Gamma_{\rm SD}^{K\to e\nu\gamma}/\Gamma_{\mu 2}$ is then calculated as a function of the W mass. The anomalous magnetic moment of W and its quadrupole moment are set equal to zero.

From the calculated branching ratio of Ref. 12 as a function of M_{W} , we obtain from the measured upper limit on the branching ratio the lower limit, $M_W > 0.95$ GeV. This limit is somewhat lower than the limit, $M_W \gtrsim 2$ GeV, obtained by high-energy neutrino experiments. 13,14

We would like to thank Dr. L. B. Auerbach, Dr. K. W. Rothe, and Dr. C. H. West for their efforts in the construction of the experimental apparatus and the analysis of the K_{e2} data, which was necessary for obtaining the $K \rightarrow e\nu\gamma$ results. D. Buchholz, H. Crothamel, and E. Mayer also contributed substantially to the design and construction of the apparatus. We wish to thank the staff of the Princeton-Pennsylvania Accelerator, where this experiment was performed, for their excellent cooperation.

PHYSICAL REVIEW D

VOLUME 1, NUMBER 5

1 MARCH 1970

Photoproduction of Electron Pairs as a Test of Quantum Electrodynamics

P. J. BIGGS, D. W. BRABEN, R. W. CLIFFT, E. GABATHULER, P. KITCHING, AND R. E. RAND Science Research Council, Daresbury Nuclear Physics Laboratory, Daresbury, Near Warrington, Lancashire, England (Received 27 October 1969)

As a test of the validity of quantum electrodynamics (QED) for heavy virtual leptons, cross sections for wide-angle electron-pair photoproduction have been measured using hydrogen and carbon targets. Electron pairs were detected in two independent mirror-image spectrometers which identified production angles and momenta. A symmetrical arrangement was used in which interference between Bethe-Heitler and virtual Compton graphs is identically zero. Data were obtained at electron production angles from 5° to 7° and momenta from 1 to 2 GeV/c, and were compared with theory by means of a Monte Carlo calculation. Up to the maximum invariant mass of the electron pair 489 MeV/c², the data are consistent with the predictions of QED for both targets, confirming the results of other recent wide-angle pair-production and bremsstrahlung experiments in this energy range. Expressing the results in terms of a cutoff parameter A, where any positive deviation from QED is proportional to $\Lambda^{-4}Q_l^{A}$ (where Q_l is the mass of the virtual lepton), one obtains $\Lambda > 0.76 \text{ GeV}/c^2 \text{ with } 95\%$ confidence. For a similar negative deviation, $\Lambda > 0.55 \text{ GeV}/c^2$.

1. INTRODUCTION

DURING the last few years a number of experiments have been performed to test the validity of quantum electrodynamics (QED). QED is, of course, the most complete of all available theories of elementary particle interactions and describes a wide range of phenomena with high accuracy. If it is pushed to extreme limits, however, in which the interaction takes place over a very short distance, it might be expected to break down. The forms of breakdown which may occur are modifications¹ of lepton or photon propagators when the particles are well off their mass shells, modification of the vertex function, and the introduction of heavy electromagnetic particles.2

These forms of modification are not strictly independent but any observed breakdowns could in practice be described in terms of one of them. The class of experiments with which we are concerned [wide-angle pair production (WAPP) and wide-angle bremsstrahlung (WAB)] is generally interpreted as testing the lepton propagator.

Much interest has been shown in this field since the original WAPP (electron) experiments at CEA3 and Cornell⁴ showed an apparently serious deviation from the predictions of QED. Subsequent similar experiments

Donald E. Neville, Phys. Rev. 124, 2037 (1961).
 S. M. Berman, A. Ghani, and R. A. Salmeron, Nuovo Cimento 25, 685 (1962).

¹³ G. Bernardini *et al.*, Nuovo Cimento **38**, 608 (1965).

¹⁴ R. Burns et al., Phys. Rev. Letters 15, 42 (1965).

¹ S. D. Drell, Ann. Phys. (N. Y.) 4, 75 (1958). ² F. E. Low, Phys. Rev. Letters 14, 238 (1965).

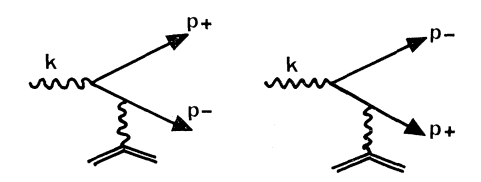
⁸ R. B. Blumenthal, D. C. Ehn, W. L. Faissler, P. M. Joseph, L. J. Lanzerotti, F. M. Pipkin, and D. G. Stairs, Phys. Rev. 144, 1199 (1966).

⁴ R. M. Talman, Bull. Am. Phys. Soc. 11, 380 (1966).

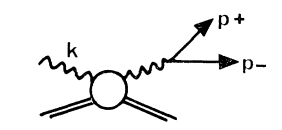
at CEA5 and DESY6 and further experiments at Cornell, however, showed agreement with QED. The experiment described here, performed at Daresbury Nuclear Physics Laboratory, confirms the results of these last three experiments, and is the first experiment performed with hydrogen.

Further confirmation for the validity of QED for electrons is provided by WAB experiments at Frascati⁸ and Cornell⁹ and for muons by a WAPP experiment at Cornell¹⁰ and a WAB experiment at Brookhaven.¹¹ Other aspects of validity of QED and electron-muon universality have been discussed recently in several review papers. 12

In the present experiment¹³ the photoproduction of wide-angle electron pairs was observed in a symmetrical arrangement using targets of carbon and hydrogen. The data agree with the predictions of QED up to the maximum electron-pair invariant mass, 489 MeV/ c^2 . Previous WAPP experiments have all been performed with carbon targets. Hydrogen was introduced in this investigation in order that the cause of any possible deviation from QED (e.g., elastic form factors, inelastic nuclear effects, Compton effect, etc.) might be identified.



(a) BETHE-HEITLER DIAGRAMS



(b) COMPTON DIAGRAMS

Fig. 1. Graphs for photoproduction of electron pairs.

⁵ K. J. Cohen, S. Homma, D. Luckey, and L. S. Osborne, Phys.

Rev. 173, 1339 (1968).

⁶ J. G. Asbury, W. K. Bertram, U. Becker, P. Joos, M. Rohde, A. J. S. Smith, S. Friedlander, C. L. Jordan, and S. C. C. Ting, Phys. Rev. 161, 1344 (1967). See also H. Alvensleben et al., Phys. Rev. Letters 21, 1501 (1968).

⁷ E. Eisenhandler, J. Feigenbaum, N. Mistry, P. Mostek, D. Rust, A. Silverman, C. Sinclair, and R. Talman, Phys. Rev. Letters 18, 425 (1967).

⁸ C. Bernardini, F. Felicetti, R. Querzoli, V. Silvestrini, G. Vignola, L. Meneghetti Vitale, and S. Vitale, Nuovo Cimento Letters 15 (1969).

⁹ R. H. Siemann, W. W. Ash, K. Berkelman, D. L. Hartill, C. A. Lichtenstein, and R. M. Littauer, Phys. Rev. Letters 22, 421

(1969).

10 S. Hayes, R. Imlay, P. M. Joseph, A. S. Kiezer, J. Knowles, and P. C. Stein, Phys. Rev. Letters 22, 1134 (1969).

11 A. D. Liberman, C. M. Hoffman, E. Engels, Jr., D. C. Imrie, P. G. Innocenti, R. Wilson, C. Zajde, W. A. Blanpied, D. G. Stairs, and D. J. Drickey, Phys. Rev. Letters 22, 663 (1969).

12 W. K. H. Panofsky, in Proceedings of the Fourteenth International Conference on High-Energy Physics, Vienna, 1968 (CERN, Geneva, 1968), p. 23. S. C. C. Ting, ibid., p. 43.

13 P. J. Biggs, D. W. Braben, R. W. Clifft, E. Gabathuler, P. Kitching, and R. E. Rand, Phys. Rev. Letters 23, 927 (1969).

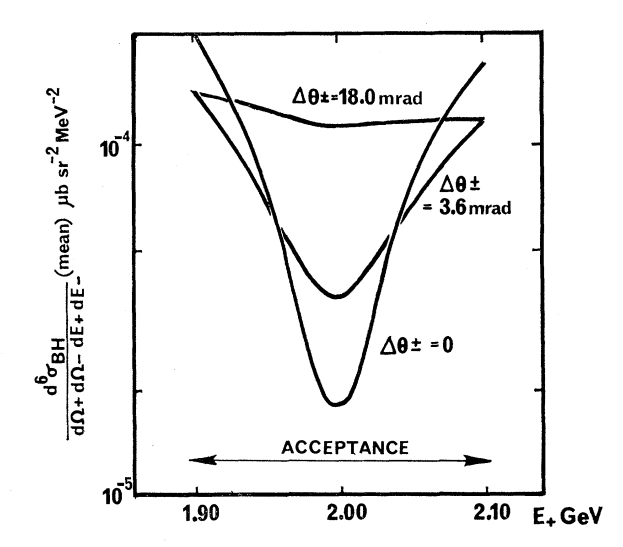


Fig. 2. Mean differential Bethe-Heitler WAPP cross section as a function of E_+ for fixed E_- and other parameters symmetrical: $\bar{E}_{-}=2$ GeV, $\bar{\theta}_{\pm}=5^{\circ}$, $\phi=0$, $\Delta E_{\pm}/E_{\pm}=0.02$, $\Delta \phi=0$. The cross section is plotted for various values of $\Delta \theta_{\pm}$: 0, 3.6 mrad (single θ counter) and 18.0 mrad (total θ acceptance).

WAPP as a test of QED was first proposed by Bjorken, Drell, and Frautschi¹⁴ (BDF), who calculated the cross section for the Bethe-Heitler¹⁵ process described by the graphs in Fig. 1(a). The contribution of the Compton graphs, Fig. 1(b), was shown to be negligible for electromagnetic couplings. Later calculations by Berman and Drell¹⁶ and Ter-Martirosyan and Boreskov¹⁷ on the ρ-dominant Compton process showed that this also was very small. It was also pointed out by BDF that under symmetric conditions of electronpositron detection, interference between the two types of graph is identically zero due to charge-conjugation invariance. A further advantage of the symmetrical arrangement is that it minimizes the 4-momentum transferred to the target nucleus, thus reducing uncertainties due to form factors. This type of experiment also tests the lepton propagator at unique mass values in the spacelike region, whereas WAB involves timelike propagators as well.

The Bethe-Heitler differential cross section as derived by BDF is

 $d^6\sigma_{\rm BH}$ $d\Omega_{+}d\Omega_{-}dE_{+}dE_{-}$

$$= \frac{\alpha^3 M}{4\pi^2} \frac{E_+ E_-}{p_+ \cdot P_i + p_- \cdot P_i - p_+ \cdot p_-} S(k) \lambda_{11}(k) , \quad (1.1)$$

¹⁴ J. D. Bjorken, S. D. Drell, and S. C. Frautschi, Phys. Rev. 112, 1409 (1958).

15 H. Bethe and W. Heitler, Proc. Roy. Soc. (London) 146, 83 (1934).

¹⁶ S. M. Berman and S. D. Drell, Phys. Rev. 133, B791 (1964). ¹⁷ K. A. Ter-Martirosyan and K. G. Boreskov, Phys. Letters 25B, 223 (1967).

TABLE I. Symbols and definitions.

=4-momentum of incident photon =maximum photon energy of bremsstrahlung beam S(k) = bremsstrahlung spectrum =initial 4-momentum of nucleus = final 4-momentum of nucleus $=P_i+P_f$ $=P_f-P_i=4$ -momentum transferred to nucleus =4-momentum of positron =4-momentum of electron =4-momentum of virtual lepton =invariant mass of electron-positron pair =angle between p_+ and k=angle between p_ and k = angle between p_+ , k plane and p_- , k plane = nuclear electric (charge) form factor = nuclear magnetic form factor = mass of nucleus =atomic number of nucleus = mass number of nucleus α = fine structure constant $\hbar = c = 1$ Metric: $a \cdot b = a_0 b_0 - \mathbf{a} \cdot \mathbf{b}$ =electron mass

where

$$\begin{split} \lambda_{11}(k) &= \frac{-1}{Q_n^4} f_1(Q_n^2) \bigg[\frac{k \cdot p_+}{k \cdot p_-} + \frac{k \cdot p_-}{k \cdot p_+} + \frac{Q_n^2 p_+ \cdot p_-}{k \cdot p_+ k \cdot p_-} \bigg] \\ &- \frac{1}{2Q_n^4} f_2(Q_n^2) \bigg[\frac{(p_+ \cdot R)^2 + (p_- \cdot R)^2}{k \cdot p_+ k \cdot p_-} \bigg], \end{split}$$

where

$$k = \frac{p_+ \cdot P_i + p_- \cdot P_i - p_+ \cdot p_-}{M - E_+ (1 - \cos\theta_+) - E_- (1 - \cos\theta_-)},$$

$$f_1(Q_n^2) = 2[G_E^2 + (Q_n^2/4M^2)G_M^2],$$

$$f_2(Q_n^2) = (4/R^2)[G_E^2 - (Q_n^2/4M^2)G_M^2].$$

Symbols are defined in Table I.

At symmetry an approximate form for the differential cross section is

$$\frac{d^6 \sigma_{\rm BH}}{d\Omega_{+} d\Omega_{-} dE_{+} dE_{-}} \simeq \frac{\alpha^3}{2\pi^2} \frac{1}{p_{\pm}^{3} \theta_{\pm}^{6}} S(k) G_{E}^{2}. \quad (1.2)$$

Further useful expressions for various invariant quantities at symmetry are

$$Q_l^2 \simeq -\frac{1}{2}k^2\theta^2, \tag{1.3}$$

$$Q_n^2 \simeq -k^2 \theta^4$$
, (1.4)

$$Q_m^2 \simeq k^2 \theta^2 \simeq -2Q_l^2. \tag{1.5}$$

Equations (1.2) and (1.3) show that in order to observe large values of Q_t^2 , it is necessary to measure very small cross sections. The design of a WAPP experiment must therefore be a compromise between the maximum value of Q_t^2 and counting rate.

An important feature of the Bethe-Heitler cross section near symmetry is the now-famous dips. Examples

of this are shown in Fig. 2, where the variation of the cross section [Eq. (1.1)] with E_+ is shown. Other parameters are fixed. Figure 2 also shows how the dip is smeared out by θ acceptances of 3.6 mrad (single θ counter) and 18 mrad (total θ acceptance) as in the present experiment. The dips are also smeared out by the other finite acceptances, as well as by multiple scattering, radiative, and bremsstrahlung effects, etc. These dips present a considerable problem in calculating the theoretical yield to be expected in a given apparatus and consequently any comparison between theory and experiment generally involves a Monte Carlo calculation. Furthermore, the extreme narrowness of the dips renders them virtually unobservable experimentally, since in a symmetric experiment with sufficiently good resolution, the statistical accuracy obtainable is poor. No attempts have been made, therefore, to trace this structure in the cross section.

2. APPARATUS

A. Spectrometers

The apparatus, consisting of two identical mirrorimage spectrometers, which may rotate about a common pivot, is shown in Fig. 3. It was designed from the points of view of flexibility and separation of the various parameters as far as possible. A bending magnet just beyond the target to separate the electron pairs (as used by other groups^{3,6}) was avoided. Such a magnet has the considerable disadvantage of mixing momentum and production angle and its field must be known very precisely since the symmetric cross section [Eq. (1.2)] is proportional to θ_{\pm}^{-6} .

Each spectrometer consisted of two half-quadrupole magnets and a bending magnet. The optical properties were as follows: (a) point to point focusing in the vertical (momentum) plane, and (b) parallel to point focusing in the horizontal (θ) plane. This permitted the use of a 300-mm-long hydrogen target. The orthogonality of the momentum and θ planes ensured the definition of production angles independently of momentum. The use of half-quadrupoles permitted the observation of production angles as small as 5°.

The acceptance of the spectrometers was defined by scintillation counters to avoid slit-scattering uncertainties, while the amount of scattering material before the bending magnet was minimized so that the effects of bremsstrahlung and multiple scattering therein could be neglected. This was achieved by using helium between the target and the first counter. The counters C_0 and C_1 (see Fig. 3) defined the vertical and horizontal acceptances, respectively. C_2 was an oversize trigger counter. The momentum counter hodoscopes M were situated in the focal planes of the spectrometers. Each consisted of five counters spanning a total momentum acceptance $(\Delta p/p) = 0.10$. The hodoscopes ϕ and θ each consisted of five counters. The horizontal angular acceptance was $\Delta \theta = 18$ mrad, the total solid angle being

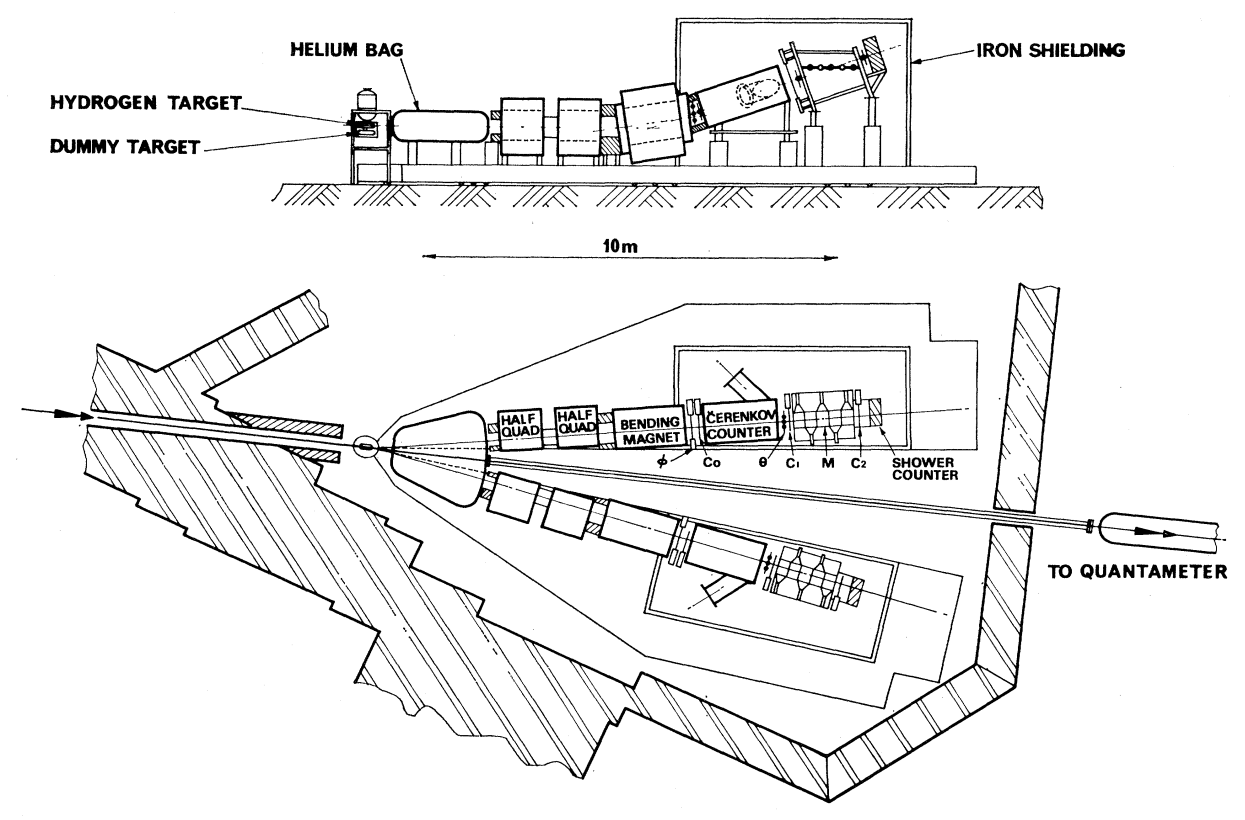


Fig. 3. Apparatus for wide-angle pair production.

 $\Delta\Omega$ =0.50 msr. The range of angles ϕ observed at one setting with θ \simeq 0.1 rad was $\Delta\phi$ \simeq 0.3 rad. None of the counters could "see" the target directly.

The counters defining the solid angle (C_0 and C_1) were of plastic scintillator (NE 102A), 6.4 mm thick, set perpendicular to the principal trajectory. Edge effects were thus very small and, for scintillator sizes of order 200 mm, contributed negligible error to the acceptance determination. The momentum counters, however, were of 10 mm thick scintillator and at an angle of $\sim 5.5^{\circ}$ to the principal trajectory. The momentum bite was not, therefore, well defined due to considerable edge effects. This quantity could, however, be estimated by observing the regions of overlap between adjacent M counters. The total correction due to this effect was 1.03 ± 0.01 for each spectrometer.

All scintillators were coupled by Lucite light guides to selected 56 AVP photomultipliers. A gallium phosphide diode "flasher" was embedded in each light guide for monitoring both the timing and amplitude of the photomultiplier pulses.

In each arm electrons were identified by a gas threshold Čerenkov counter and a shower counter. The Čerenkov counters contained Freon 12 at a pressure of 0.8 atm and were sensitive to electrons of energy greater than 14 MeV. The total path length of particles in the gas was ~ 2 m. Čerenkov light was focused by a concave

mirror (formed under pressure from Lucite and aluminized) onto the face of an RCA 4522 photomultiplier. The shower counters¹⁸ each consisted of 12 slabs of lead, each one radiation length thick, interspersed with sheets of Lucite 10 mm thick. The edges of the Lucite sheets were cemented to a single slab of Lucite, 25 mm thick, which was viewed by two RCA 4522 photomultipliers. The Čerenkov and shower counters were also equipped with diode flashers.

B. Targets

The hydrogen target was of the condensation type and consisted of two identical cells, one full and one empty for background measurements. Each cell was a cylinder of H film 300 mm long \times 50 mm diameter with beam windows 0.1 mm thick. End caps of the cells were preformed under pressure and cemented with Epoxy to the cylindrical bodies. The hydrogen reservoir and cells were "superinsulated" by many layers of aluminized Mylar (suitably reduced to an acceptable thickness on the beam windows). The total thickness of Mylar intersected by the beam (including the vacuum windows) was \sim 0.5 mm.

The target was aligned through a viewing port to high accuracy. Its length was measured optically at the

¹⁸ C. A. Heusch and C. Y. Prescott, IEEE Trans. Nucl. Sci. 4, 213 (1965).

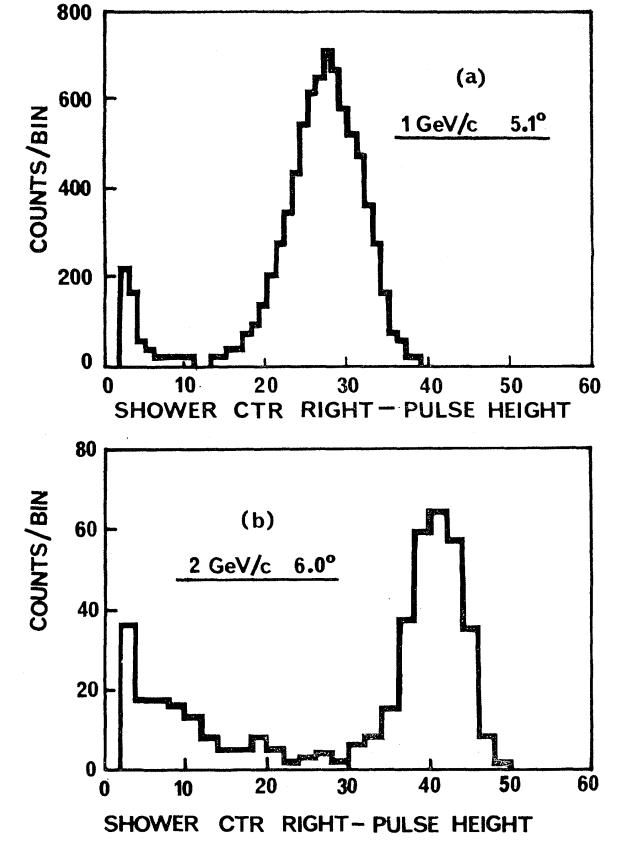


Fig. 4. Pulse-height distributions for single electrons (as defined by the Čerenkov counter) incident on the right-hand shower counter. The electrons were photoproduced from hydrogen at (a) 1 GeV/c and θ =5.1°, and (b) 2 GeV/c and θ =6.0°. See text for further details.

working temperature in vacuum but with the aluminized Mylar removed. The density of liquid hydrogen at atmospheric pressure was taken as 70.8 kg m⁻³.

Carbon targets were of high-purity and high-density graphite (1700 kg m⁻³) 10 and 20 mm thick.

C. Photon Beam

The photon beam was produced by steering the circulating electron beam in NINA onto a tungsten target 0.15 radiation lengths thick. The emergent beam was collimated to produce a spot size 15×15 mm at the target and cleared of charged particles by two orthogonal bending magnets. Before each run the beam line was surveyed optically and the alignment was checked by "photographing" the photon beam at the target and quantameter. The beam was monitored by a Wilson¹⁹ type of quantameter that was calibrated²⁰ in an electron beam against a Faraday cup to an accuracy of $\pm 0.8\%$. Photon intensities of $\sim 10^{11}$ equivalent quanta per second were obtained at electron energies $\geqslant 4$ GeV. No

evidence of saturation effects in the monitor was found throughout the experiment.

D. Magnet Calibration

The magnets were calibrated separately by means of a Hall probe (calibrated in turn by nuclear magnetic resonance) that was mounted on a device which automatically scanned the useful field volume and printed out readings for a selected matrix of positions. From these readings the mean magnetic lengths of the magnets and maximum field values as a function of magnet current were obtained. It was found that field configurations could be reproduced to an accuracy of better than 0.1% without careful recycling of the magnets, although a standard procedure was in fact used.

Several trajectories were also traced through each magnet using a floating wire apparatus which employed an air-bearing pulley and accurate (0.01 mm) traveling microscopes. The use of an aluminum wire 0.13 mm in diameter with nylon thread "leaders" and tensions of the order 200 g wt ensured that corrections due to the weight and stiffness of the wire, friction, etc., were negligible.

A ray-tracing program was used in conjunction with the probe measurements, to compare them to the floating-wire results. The over-all accuracy of probe and ray-tracing procedures was $\pm 0.1\%$ for bending magnets and $\pm 0.15\%$ for quadrupoles. The floating-wire method was accurate to $\pm 0.15\%$. In each case it was found that the values of $\int B \cdot dl$ given by the two methods agreed to within 0.15%, giving some confidence in the methods employed. In each method the limiting factor was in measuring the position of the probe or wire. The actual field measurements by the Hall probe were accurate to 0.01%.

The optical properties of the spectrometers were optimized and calculated using first-order transport theory. Second- and third-order corrections for the complete system were then calculated using the ray-tracing program. Again accuracy of the over-all system was limited by surveying errors to $\sim \pm 0.1\%$.

E. Counter Efficiencies

The efficiencies of all scintillation counters (normally set with plateaux of at least 6 dB) were measured with a small defining counter and found to be $\geq 99.7\%$ in all cases.

The efficiencies of the Čerenkov and shower counters were found by scattering an electron beam into the spectrometers and also by observing 0° electron pairs directed into the spectrometers by a bending magnet at the target. The Čerenkov counters were found to be $\geq 99.7\%$ efficient with a resolution of $\sim 60\%$ at all energies, while the efficiency of the shower counters was 99% at 1 GeV and 100% at energies > 1.5 GeV.

A knowledge of the efficiencies of the selecting devices for detecting pions is vital in any WAPP experiment.

 ¹⁹ R. R. Wilson, Nucl. Instr. 1, 101 (1957).
 ²⁰ N. R. S. Tait, Daresbury Nuclear Physics Laboratory, Internal Communication, 1968 (unpublished).

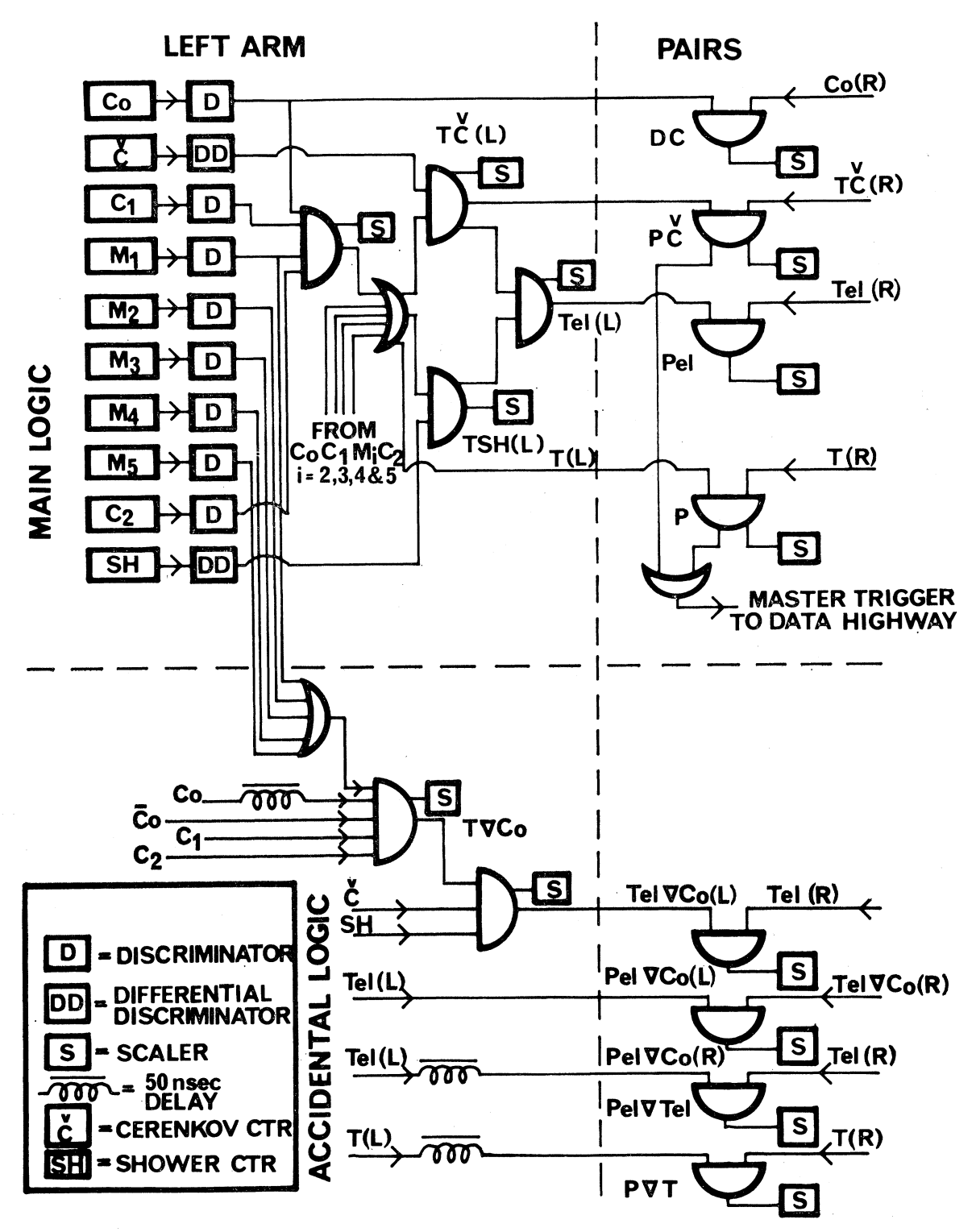


Fig. 5. Simplified schematic diagram of logic system. The delay symbol ∇ is defined as follows: If the pulse $A \equiv B_1 \cdot B_2 \cdot \cdots \cdot B_r \cdot \cdots \cdot B_n$, then $A \nabla B_r \equiv B_1 \cdot B_2 \cdot \cdots \cdot B_r$ (delayed) $\cdot \cdots \cdot B_n$.

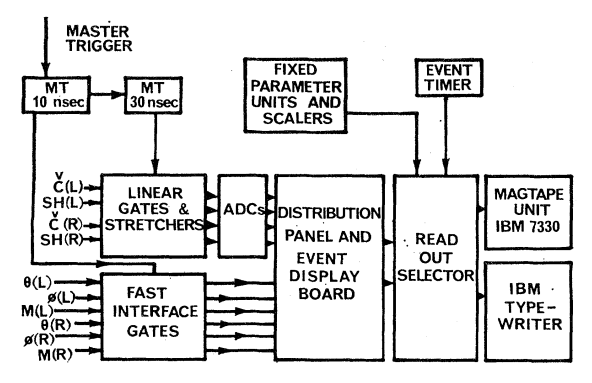


Fig. 6. Data highway.

These were measured by setting the spectrometers at $\theta \simeq 11^{\circ}$ and $p \simeq 2 \text{ GeV}/c$ where the π -pair rate from ρ decay is the dominant process. The electron-pair rate is negligible. Pion efficiencies could then be measured by observing apparent π -e coincidences and comparing with the π - π rate. The Čerenkov counters were found to have a pion efficiency of 2×10^{-3} , while the shower counters, when biased for 1-GeV/c electrons, showed pion efficiencies of ~ 0.05 . Thus the over-all efficiency of the apparatus to π pairs was $(2 \times 10^{-3})^2 \times (0.05)^2 = 10^{-8}$. Since, at the smaller angles employed to observe electron pairs, the π -pair rate was never greater than 5×10^3 times the electron rate, the rejection was adequate.

However, the main contamination of the data was not due to pions. It was found that even with a very low pion background the single-arm Čerenkov counter rates were always ~15% higher than the shower counter rates. The effect is attributed to arbitrary electrons producing showers in the magnet poles and possibly elsewhere. Low-energy electrons from these showers could trigger the Čerenkov counter, but only a fraction of the total energy of the shower reached the shower counter and was insufficient to record a count. This theory is supported by the high correlation between this type of event and multiple hodoscope events. This process is illustrated by the pulse-height distributions for the right-hand shower counter at particle momenta 1 and 2 GeV/c shown in Figs. 4(a) and 4(b), respectively. These distributions were obtained by observing single particles photoproduced from hydrogen, at the angles stated, and selected by the Čerenkov counter. The low-energy tails due mainly to the shower electrons are easily seen, although even in this "single-arm" mode of operation the separation of the good events is adequate. The energy selecting property of the shower counters was thus very important in "cleaning up" the spectrometers.

F. Logic and Data Highway

A simplified diagram of the logic system is shown in Fig. 5. This system was built up from Edgerton,

Germeshausen and Grier²¹ modules. Single-arm events (T) were defined by a fourfold coincidence between the counters C_0 , C_1 , C_2 , and M_i , where the last is any counter in the momentum hodoscope. Such events were monitored in coincidence with the Čerenkov counter $(T\check{C})$ and shower counter (TSh) separately, and both together (Tel). Pair events (P), "Čerenkov pairs" $(P\check{C})$, and "electron" pairs (Pel) were defined by appropriate coincidences between pulses from the two arms with resolving times of 5 nsec.

For pair events defined by P or PČ, the hodoscope information $(M_L,\phi_L,\phi_L,M_R,\theta_R,\phi_R)$, pulse heights of Čerenkov and shower counters, instantaneous machine energy, and time interval (resolving time 1 nsec) between the single-arm events were recorded on magnetic tape via the data highway shown in Fig. 6. This information was used to make the final selection of electron-pair events. The same information was displayed on a board for each event so that a continuous check of the system could be made during a run.

The duty cycle of the machine was monitored by observing random coincidences (DC) between the two C_0 counters (only a negligible number of these were due to true pairs).

A thorough study was made of the accidental coincidences possible in the system. As well as the obvious "arm-to-arm" accidentals (monitored as shown in Fig. 5), there were significant contributions from random events in which, for instance, 11 out of the 12 counters recorded a true pair of particles, one of which did not traverse the 12th counter. This pair could form an accidental coincidence with the high singles rate of the 12th counter. Such events were checked in all possible counter combinations. It was found that the main contribution was due to the C_0 counters. Random events with C_0 delayed (but vetoed in the main coincidence) were therefore continuously monitored as shown in Fig. 5. Other contributions were calculated from the rates for the various counter combinations.

Relative resolving times of the direct and accidental channels were measured in order to calculate the true accidental rates. Absolute resolving times were measured as an additional check by observing random coincidences between pulses in a single counter (e.g., C_0), due to particles from a radioactive source, with "flasher pulses" in the remaining counter (e.g., C_1 , C_2 , M_i). Pulses due to the flashers were also invaluable for periodically checking the stability of the system.

Dead time in the system was significant and had to be measured carefully. The limiting components in this respect were the discriminators which had dead times of up to 20 nsec. The method by which these dead times were measured is illustrated schematically in Fig. 7(a). The clipped but nonstandardized pulse from a counter x is split and delayed in one branch of the circuit before the two pulses are again mixed. (The factor of 2 in pulse height lost by this circuit is compensated by adjusting the appropriate attenuator.) The discriminator is

²¹ Edgerton, Germeshausen, and Grier, Inc., Nuclear Instrumentation Division, Salem, Mass.

triggered by the undelayed pulse and will not respond to the second delayed pulse for a certain range of delay. The output from the discriminator is put in coincidence with the standard pulse from a group of counters y, also delayed by the same time as the delayed pulse from x. As the delay is varied, the counting rate from the coincidence unit shows the variation illustrated in Fig. 7(b). From this curve, the dead time may be calculated. The measurement is, of course, made $in\ situ$, the logic being disturbed as little as possible

Total dead-time corrections in the system were up to 5%. These were compensated by accidental corrections of up to 10%, giving a maximum total counting rate correction of $\sim 5\%$.

3. EXPERIMENTAL PROCEDURE

With the spectrometers set symmetrically about the photon beam direction and the corresponding magnets at the same polarities, single-arm electron and pion rates were recorded. The corrected rates for the two arms always agreed to within 1%, providing a sensitive check on the stability of the system.

In order to check the alignment and optics of the spectrometers, both pair and single-arm yields were measured for a thin carbon target at various positions along the beam line. The effect of moving a lead stop across the front of each spectrometer aperture was also observed. In each case the results agreed with the predictions of the Monte Carlo calculation described below (see Sec. 4 A).

Electron pairs from hydrogen were recorded at average production angles of 5.1° , 6.0° , and 7.0° and for electron momenta of 1.0, 1.5, and 2.0 GeV/c. Data were also taken with carbon at some of these settings.

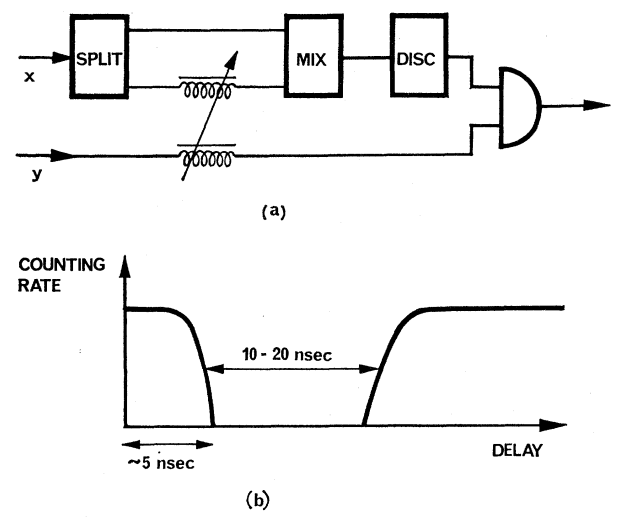


FIG. 7. (a) Schematic circuit for measuring discriminator dead time $in \ situ$. The dead time due to the undelayed pulse is clearly seen in plots such as (b), where the output from the coincidence unit is plotted against delay. x represents the clipped pulse from a single counter. y is a standard pulse from a group of counters normally used in coincidence with x.

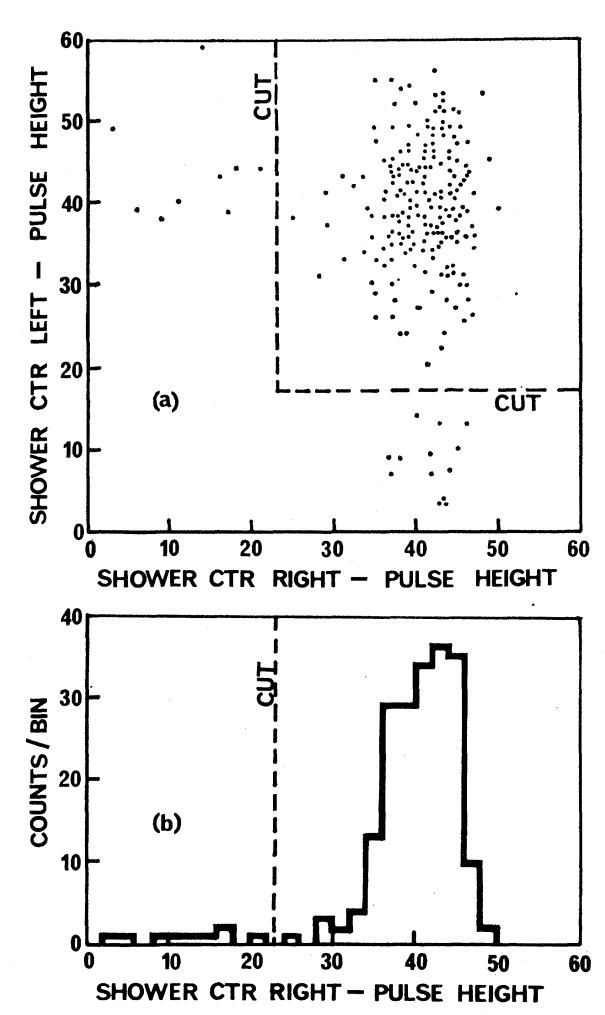


Fig. 8. (a) Distribution of left/right shower-counter pulse heights for symmetric electron pairs (as defined by the Čerenkov counters) photoproduced from hydrogen at 2 GeV/c and 6° . The region of good events with both pulse heights above the cuts is clearly distinguished. (b) The distribution of pulse heights in the right-hand shower counter for the same events.

Background rates for the hydrogen target were measured using the dummy cell after initially checking that both cells produced the same rate when empty. The correction to the hydrogen data was about 19%. The carbon targets were mounted in air which produced a background rate of a few percent. This was large enough to require correction but difficult to measure by observing electron pairs. The effective thickness of the air target was therefore deduced from the single-arm electron rates using carbon targets both 10 and 20 mm thick to take account of the considerable t^2 effect (see Sec. 5 A).

All data were taken at a constant ratio of $k/k_{\rm max}$ equal to 0.87 to facilitate the calculation of radiative corrections and minimize the effect of systematic errors. Half the data were taken at each polarity of the spectrometers to eliminate interference effects due to possible asymmetries.

Possible candidates for electron-pair events were examined using the magnetic-tape information. Events were accepted on the criteria of pulse heights in the various counters, hodoscope patterns, and timing. Figure 8 shows typical shower-counter pulse-height distributions for particle pairs, defined by PČ, produced from hydrogen at 2 GeV/c and 6°. The region in which both particles in the pair are electrons of the correct energy is clearly seen in Fig. 8(a). If the distribution 8(b) is compared with that shown in Fig. 4(b), it can be seen that pair events defined by the Čerenkov counters are much cleaner than the corresponding single-arm events. The uncertainty due to showering of arbitrary electrons in the spectrometer is thus negligible in the pair data, and such events were easily rejected. Events were also rejected if more than two counters fired in any of the angle hodoscopes. Those events with two counters in one hodoscope showed distributions consistent with δ rays being produced by the incident particle and were not rejected. On the average, 2% of Pel events were rejected by pulse-height criteria, while approximately 0.3% more were rejected purely because of their hodoscope patterns. Counting rate and background corrections were made appropriately.

4. COMPARISON WITH THEORY

A. Monte Carlo Calculation

As explained in Sec. 1, the rapid variation of the Bethe-Heitler cross section over the acceptance of the apparatus necessitated the calculation by a Monte Carlo method of the electron-pair yields to be expected theoretically. These could then be compared with the experimental yields.

The theoretical yields were determined by evaluating the sixfold integral:

$$Y = (E.Q.) \frac{N_0 \rho t}{A} \int \int \int \int \int \int dE_+ dE_- d\Omega_+ d\Omega_-$$

$$\times \left[A_+(\mathbf{p}_+, \mathbf{r}) A_-(\mathbf{p}_-, \mathbf{r}) \frac{d^6 \sigma_{\rm BH}}{dE_+ dE_- d\Omega_+ d\Omega_-} \right],$$

where E. Q. is the number of equivalent quanta, N_0 is Avogadro's number, ρ is the target density, and t is the target thickness.

 $A_{+}(\mathbf{p}_{+},\mathbf{r})$ and $A_{-}(\mathbf{p}_{-},\mathbf{r})$ are the acceptance functions for the individual spectrometers for particles that are created at position \mathbf{r} in the target, travelling with 3-momentum \mathbf{p}_{\pm} . The quantities A_{\pm} are equal to unity or zero depending on whether or not the particles successfully traverse the spectrometer (i.e., are within the acceptance). These functions include effects of multiple scattering and bremsstrahlung.

The integral was evaluated by writing it in a Monte Carlo form:

$$Y = (E.Q.) \frac{N_0 \rho t}{A} \frac{\Delta E_+ \Delta E_- \Delta \phi_+ \Delta \phi_- \Delta (\cos \theta_+) \Delta (\cos \theta_-)}{n}$$

$$\times \sum_{i=1}^{n} \left[A_{+}(\mathbf{p}_{+}(i),\mathbf{r}(i)) A_{-}(\mathbf{p}_{-}(i),\mathbf{r}(i)) \frac{d^{6}\sigma_{\mathrm{BH}}}{dE_{+}dE_{-}d\Omega_{\perp}d\Omega_{-}} \right]$$

where the ranges ΔE_{\pm} , $\Delta \phi_{\pm}$, $\Delta (\cos \theta_{\pm})$ are greater than the spectrometer acceptances and the sum is evaluated for n independent events randomly chosen within these limits. The procedure in evaluating Y is as follows:

For each of n events:

- (a) Generate random position in target.
- (b) Generate random E_+ , ϕ_+ , $\cos\theta_+$ within the specified limits.
- (c) Track the positive particle through the spectrometer using first-order transport theory with second- and third-order corrections where necessary. Loss of particles by multiple scattering in the target and various scintillators, etc., is also included at this stage (see below).

Hence $A_{+}=1$ or 0.

- (d) If $A_{+}=1$, repeat (b) and (c) for negative particle. Hence $A_{-}=1$ or 0.
- (e) If $A_-=1$, calculate $d^6\sigma_{\rm BH}/dE_+dE_-d\Omega_+d\Omega_-$ and add to sum.

Hence the yield Y is calculated.

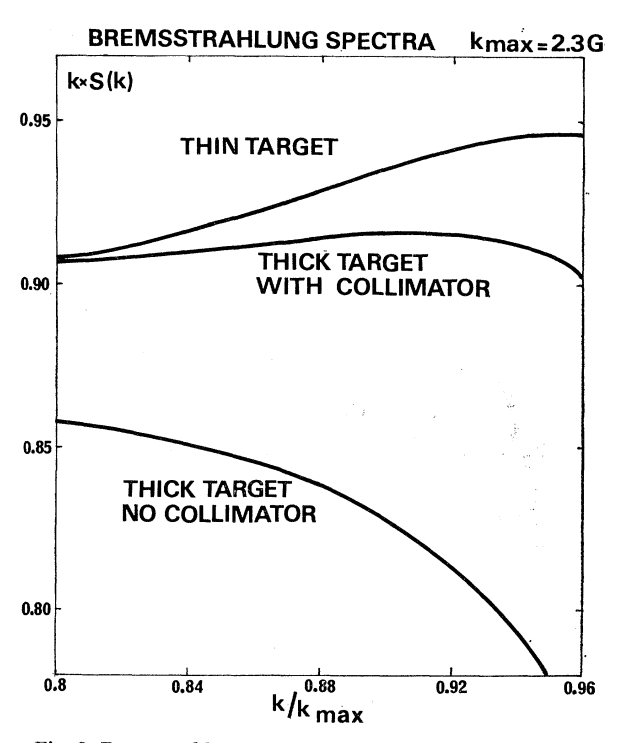


Fig. 9. Bremsstrahlung spectra for $k_{\rm max}\!=\!2.3$ GeV for thin and 0.15-radiation-length-thick tungsten targets. The effect on the spectrum of the experimental collimator is also shown. The curves are normalized to have the same total area (=one equivalent quantum).

Multiple scattering of the electron and positron in the target and spectrometers was calculated using the theory of Nigam, Sundaresan, and Wu. 22 This theory, which is similar to that of Molière 23 but more correct for electrons, treats the scattering of a relativistic particle of spin $\frac{1}{2}$ in a screened atomic field up to second-order Born approximation. The total spatial and angular distributions are obtained as a sum of polynomial terms. The dominant three terms were put in the program in tabular form. Calculation of multiple scattering in the target was simplified by dividing its thickness into five parts and classifying each event according to its production position in the target.

Since all counters except those defining the acceptance were made oversize, it was possible for both in-scattering and out-scattering to occur. The net multiple scattering losses were thus very small. At 1 and 2 $\,\mathrm{GeV}/c$, total losses due to multiple scattering were approximately 6 and 3%, respectively.

The predicted effects of multiple scattering were checked experimentally by inserting extra material into the spectrometer behind the bending magnet.

B. Bremsstrahlung Spectrum

The calculation of the thick-target bremsstrahlung spectrum with collimator effects was undertaken by Tait.24 This work is based on that of Tsai and Van Whitis²⁵ and calculates the thick-target photon spectrum by integration, taking into account energy loss and multiple scattering of the electrons in the target, as well as second generation effects. Figure 9 shows an example of the calculation for $k_{\text{max}}=2.3$ GeV and tungsten targets of negligible thickness (thin target) and 0.15 radiation lengths (thick target). Also shown is the effect of introducing the experimental collimator into the beam. This enhances the high-energy end of the spectrum, since the collimator selects photons produced in the forward direction rather than those produced by electrons which have undergone multiple scattering and energy loss. The calculation assumes a circular collimator, whereas the experimental collimator was in fact rectangular.

Under selected conditions the theoretical spectrum has been verified experimentally using a simple pair spectrometer.²⁶ From these measurements an estimate has been made of the effective internal target thickness. It was found to be 0.15 radiation lengths. The accuracy of this calculation in the region of interest is estimated to be $\pm 0.5\%$.

C. Nuclear Form Factors

The form factors used in evaluating the yields were taken from the following sources.

For the proton, the 3-pole fit of Hughes *et al.*²⁷ was used, this being the most accurate in the low (nuclear) momentum transfer region of this experiment $\lceil |Q_n^2| \le 4 \times 10^{-4} \text{ (GeV/}c)^2 \rceil$. In this analysis, the form factors of the proton are written in terms of the isoscalar (G_S) and isovector (G_V) nucleon form factors, i.e.,

$$G_{Ep} = G_{ES} + G_{EV}$$
, $G_{Mp} = G_{MS} + G_{MV}$.

These form factors were fitted to elastic electron scattering data assuming vector-meson dominance:

$$G_S \propto rac{a_1}{1 - Q_{n^2}/m_{\omega^2}} + rac{a_2}{1 - Q_{n^2}/m_{\phi^2}} + 1 - a_1 - a_2,$$
 $G_V \propto rac{a_3}{1 - Q_{n^2}/m_{
ho^2}} + 1 - a_3,$

where a_1 , a_2 , and a_3 are arbitrary constants, m_{ω} , m_{ϕ} , and m_{ρ} are the masses of the vector mesons φ , φ , and ρ , respectively, and m_{ρ} is treated as a free parameter.

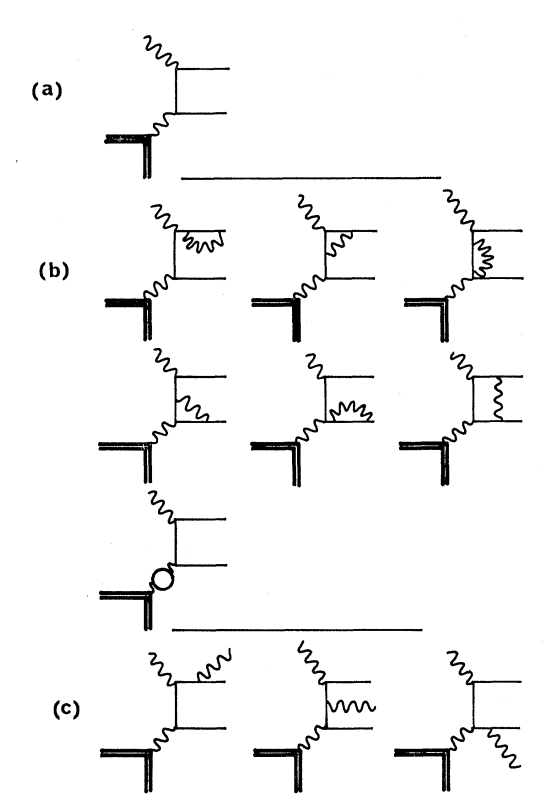


Fig. 10. Classes of graph for (a) the Bethe-Heitler process, (b) electron-pair production with one extra virtual photon, and (c) electron-pair production with the emission of a real photon.

 $^{^{22}\,\}mathrm{B.~P.~Nigam,~M.~K.}$ Sundaresan, and T.-Y. Wu, Phys. Rev. 115, 491 (1959).

 ²³ G. Molière, Z. Naturforsch. 2a, 133 (1947); 3a, 78 (1948).
 ²⁴ N. R. S. Tait, Nucl. Instr. Methods 67, 56 (1969). The authors are greatly indebted to Dr. Tait for calculating the bremsstrahlung spectrum for the conditions of this experiment.

²⁵ Y. S. Tsai and Van Whitis, Phys. Rev. 149, 1248 (1966).

²⁶ W. R. Rawlinson (private communication).

²⁷ E. B. Hughes, T. A. Griffy, M. R. Yearian, and R. Hofstadter, Phys. Rev. 139, B485 (1965).

Table II. Radiative and bremsstrahlung corrections. Corrections Δ are defined by $d\sigma_{\mathrm{pair}} = d\sigma_{\mathrm{BH}}(1-\Delta)$.

Target	<i>θ</i> (deg)	$egin{array}{c} ext{Momentum} \ ext{(GeV}/c) \end{array}$		Bremsstrahlung correction (%)
H (300 mm)	5.1	1.0	5.1	9.8
	5.1	1.5	5.3	9.8
	5.1	2.0	5.5	9.8
	6.0	1.0	4.5	9.3
	6.0	1.5	4.7	9.3
	6.0	2.0	4.9	9.4
	7.0	2.0	3.6	8.5
C (10 mm)	5.1	1.0	5.1	11.0
	5.1	1.75	5.6	11.1
	6.0	1.75	5.0	10.6
	7.0	2.0	4.0	9.9

Following Blumenthal *et al.*,³ the carbon form factor was written as a sum of elastic and quasi-elastic terms:

$$G_E^2 \simeq Z^2 F_c^2 + Z(1 - F_c^2) G_{En^2}$$
.

The elastic charge form factor F_{σ} was evaluated using the approximate harmonic-oscillator shell-model formula:

$$F_c = \{1 + \lceil (Z-2)/6Z \rceil a_0^2 Q_n^2\} \exp(\frac{1}{4}Q_n^2 a_0^2).$$

The value of the parameter a_0 as given by Crannell²⁸ was used, viz., $a_0=1.635$ fm.

D. Radiative Corrections

Higher-order or radiative corrections to the Bethe-Heitler cross sections were calculated in detail. Figure 10 shows a generalized graph for the Bethe-Heitler process at (a), graphs containing one extra virtual photon at (b), and graphs with a real photon emitted at (c). Taking these graphs into account, the cross section for electron-pair production can be written as

$$d\sigma_{\text{pair}}(E_{+}, E_{-}) = d\sigma_{\text{BH}}(E_{+}, E_{-}) + d\sigma_{\text{virt}}(E_{+}, E_{-}) + d\sigma_{\text{real}}(E_{+}, E_{-}), \quad (4.1)$$

where each quantity $d\sigma$ refers to a sixfold differential cross section.

 $d\sigma_{\rm BH}$ is of the order α^3 , while the other terms are of the order α^4 . $d\sigma_{\rm virt}$ is due to interference between the Bethe-Heitler and virtual photon graphs, while $d\sigma_{\rm real}$ is due entirely to the real photon emission. The latter contributes to the experimental yield both because the apparatus has finite acceptance and because photon energies extend up to the maximum energy available from the accelerator.

The cross sections $d\sigma_{\text{virt}}(E_+, E_-)$ and $d\sigma_{\text{real}}(E_+, E_-)$ are both divergent, but by writing

$$d\sigma_{\text{real}} = d\sigma_{\text{real, soft}} + d\sigma_{\text{real, hard}}$$

where $d\sigma_{\text{real, soft}}$ contains only contributions from emission of real photons with energies up to an arbitrary

value $\delta \ll m_e$, one can write $[d\sigma_{\text{virt}}(E_+, E_-) + d\sigma_{\text{real, soft}}]$ in a nondivergent form. The following formulas for these cross sections have been calculated by Huld²⁹ using the peaking approximation:

$$d\sigma_{\text{virt}}(E_{+},E_{-}) + d\sigma_{\text{real, soft}}(E_{+}E_{-})$$

$$= \frac{2\alpha}{\pi} \left[\left(\ln \frac{Q_{m^{2}}}{m_{e^{2}}} - 1 \right) \left(\frac{13}{12} - \frac{1}{2} \ln(E_{+}E_{-}) + \ln \delta \right) - 3 + \frac{1}{3} \ln \frac{Q_{m^{2}}}{4k^{2}} \right] d\sigma_{\text{BH}}(E_{+},E_{-}), \quad (4.2)$$

$$d\sigma_{\text{real, hard}}(E_{+}, E_{-}) = -\frac{\alpha}{\pi} \int_{\delta}^{\Delta k} \frac{dl_{0}}{l_{0}} [a_{+} d\sigma_{\text{BH}}(E_{+} + l_{0}, E_{-}) + a_{-} d\sigma_{\text{BH}}(E_{+}, E_{-} + l_{0})], \quad (4.3)$$

where

$$a_{\pm} = \frac{E_{\pm} + l_0}{E_{\pm}} \bigg\{ \bigg[1 + \frac{1}{2} \frac{l_0^2}{E_{+}^2} \bigg(\frac{E_{\pm}}{E_{+} + l_0} \bigg) \bigg] \ln \frac{Q_{m^2}}{m_e^2} - 1 \bigg\} \; ,$$

 l_0 = energy of photon emitted, and $\Delta k = k_{\text{max}} - E_+ - E_-$. Lomon³⁰ has given similar expressions.

The lower limit of the integral in Eq. (4.3) obviously cancels with the δ -dependent term in Eq. (4.2), for δ sufficiently small, so that the total cross section, Eq. (4.1), is independent of δ .

The corrections have been calculated for the conditions of this experiment using numerical integration. The results are shown in Table II.

E. Bremsstrahlung Corrections

When dealing with electrons one has to take account of their loss of energy by radiation in the fields of nuclei (bremsstrahlung) while traversing the target. The correction due to this effect was calculated on the assumption that only one photon per electron pair is produced.

The probability of an electron of initial energy (E_0) radiating a photon of energy l_0 in the target may be written

$$dp(E_0,E) = \frac{dl_0}{l_0} \frac{E}{E_0} \left[(\Gamma_1 - \Gamma_2) + \frac{1}{2} \frac{l_0^2}{EE_0} \Gamma_1 \right],$$

where Γ_1 and Γ_2 are functions characteristic of the target material and $E_0 = E + l_0$. For the case of complete screening, one can relate these functions to the effective length (in radiation lengths) of the target, $t_{\rm rad}$ of the following way:

$$t_{\text{rad}}^{\text{eff}} = \frac{1}{E_0} \int_0^{E_0} l_0 dp(E_0, E) = \frac{1}{2} (\Gamma_1 - \Gamma_2) + \frac{1}{6} \Gamma_1.$$

Under the same assumption, $\Gamma_2 = \frac{1}{3}\Gamma_1$.

²⁸ H. Crannell, Phys. Rev. 148, 1107 (1966).

B. Huld, Phys. Letters 24B, 185 (1967).
 E. Lomon, Phys. Letters 21, 555 (1966).

The total cross section for the production of electron pairs may now be written

$$d\sigma(E_{+},E_{-}) = \int_{0}^{\Delta k} d\sigma_{\text{pair}}(E_{+} + l_{0}, E_{-}) dp(E_{+} + l_{0}, E_{+})$$

$$+ \int_{0}^{\Delta k} d\sigma_{\text{pair}}(E_{+}, E_{-} + l_{0}) dp(E_{-} + l_{0}, E_{-}). \quad (4.4)$$

These integrals are again divergent because only the real photon graphs for electron nuclear scattering have been considered. If one also considers the appropriate virtual photon diagrams, divergences cancel and one obtains a correction to the Bethe-Heitler cross section:

$$d\sigma_{\text{brems}}(E_{+},E_{-}) = \frac{4}{3}l_{\text{rad}}^{\text{eff}} \left(\ln \frac{\delta^{2}}{E_{+}E_{-}} + \int_{\delta}^{\Delta k} \frac{dl_{0}}{l_{0}} \frac{E_{+}}{E_{+} + l_{0}} d\sigma_{\text{BH}}(E_{+} + l_{0}, E_{-}) + \int_{\delta}^{\Delta k} \frac{dl_{0}}{l_{0}} \frac{E_{-}}{E_{-} + l_{0}} d\sigma_{\text{BH}}(E_{+}, E_{-} + l_{0}) \right), \quad (4.5)$$

where, in this case, the average value of $t_{\rm rad}^{\rm eff}$ is half the full target thickness. This correction has been numerically integrated for this experiment, in a similar manner to the radiative corrections. Values are shown in Table II.

An alternative approach to the bremsstrahlung correction is to evaluate Eq. (4.4) directly using the Monte Carlo method described above. This may be achieved if dp is replaced by the w function of Heitler³¹:

$$w(y)dy = \frac{e^{-y}y^{b-1}}{\Gamma(b)}dy,$$

where $b=2t_{\rm rad}^{\rm eff}/\ln 2$ and y is given by $l_0=E_0(1-e^{-y})$, and where

$$\int_0^\infty w(y)dy = 1.$$

Using this formula, the results obtained for the bremsstrahlung corrections are in good agreement with those obtained from Eq. (4.5). However, it is difficult to obtain high accuracy with this method since the Monte Carlo program becomes extremely inefficient and statistics are poor. The results of Eq. (4.5) were therefore used in the final analysis.

An experimental check of the bremsstrahlung corrections was provided by data taken for two thicknesses of carbon target at the same settings. After corrections these data were consistent within the experimental and statistical errors.

It should be emphasized that all the corrections discussed above depend on the photon spectrum S(k).

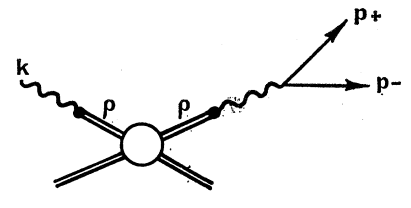


Fig. 11. ρ -dominance contribution to WAPP by the virtual Compton process.

Maintaining a constant ratio $(k/k_{\rm max})$ throughout the experiment ensured that the corrections did not vary much between settings and that any systematic errors in these calculations would be approximately the same for all settings.

F. Virtual Compton Correction

Reference has already been made to calculations^{16,17} of the WAPP yield to be expected from the Compton graph of Fig. 1(b). This process is dominated by the ρ meson as shown in Fig. 11. The ρ -nucleus scattering process is predominantly diffractive for ¹²C and for hydrogen in the forward direction.^{32,33}

Ter-Martirosyan and Boreskov¹⁷ give the following formula for the cross section due to this process at symmetry:

$$\begin{split} \frac{d^5\sigma}{dE_+d\Omega_+d\Omega_-} &= \frac{\alpha^2}{16\pi\gamma_\rho^2} \\ &\qquad \times \frac{k}{Q_m^2 \left[(1-Q_m^2/m_\rho^2)^2 + (\Gamma_\rho/m_\rho)^2 \right]} \frac{d\sigma_\rho}{d\Omega} (0^\circ) \,, \end{split}$$

where $(e/2\gamma_{\rho})$ is the ρ - γ coupling constant, Γ_{ρ} is the width of the ρ resonance, and $d\sigma_{\rho}/d\Omega(0^{\circ})$ is the differential cross section for ρ photoproduction in the forward direction. Berman and Drell¹⁶ give a cross section approximately equal to twice that given by this expression.

This cross section was evaluated for the experimental acceptance using a branching ratio for the process $\rho \to e^+e^-$ equal³⁴ to 6×10^{-5} . This quantity is related to the coupling constant γ_ρ by

$$(B.R.)_{\rho \to e^+e^-} \simeq \frac{\alpha^2}{\gamma_o^2/4\pi} \frac{m_\rho}{12\Gamma_o}$$

p. 270.

²⁴ S. C. C. Ting, in *Meson Spectroscopy*, edited by C. Baltay and A. H. Rosenfeld (W. A. Benjamin, Inc., New York, 1968).

³¹ W. Heitler, *The Quantum Theory of Radiation* (Oxford University Press, London, 1954), 3rd ed.

³² L. J. Lanzerotti, R. B. Blumenthal, D. C. Ehn, W. L. Faissler, P. M. Joseph, F. M. Pipkin, J. K. Randolph, J. J. Russell, D. G. Stairs, and J. Tenenbaum, Phys. Rev. Letters 15, 210 (1965); L. J. Lanzerotti, Ph.D. thesis, Harvard University, 1965 (unpublished); J. G. Ashbury, U. Becker, W. K. Bertram, P. Joos, M. Rohde, A. J. S. Smith, C. L. Jordan, and S. C. C. Ting, *ibid*. 19, 865 (1967).

³⁸ F. M. Pipkin, in Proceedings of the Third International Symposium on Electron and Photon Interactions at High Energies, Stanford Linear Accelerator Center, 1967 (Clearing House of Federal Scientific and Technical Information, Washington, D. C., 1968), p. 270.

TABLE III. Corrections and systematic errors.

Target effects	Correction to experimental yield (%) H (300 mm) C (20 mm)		Systematic probable error (%) H (300 mm) C (20 mm)		
Radiative Bremsstrahlung Multiple scattering (from Monte Carlo calc.) Background subtraction Absorption of photons	$ \begin{array}{c} $	$ \begin{array}{r} $	0.5 0.5 0.5 1.0 1.9 <0.2		
Spectrometer e ⁺ annihilation (0.2–0.4%) Multiple scattering (4% at 1. Definition of aperture and mo Counter efficiencies: shower momen others Quantameter calibration Bremsstrahlung spectral shap Counting rate corrections (~ Total systematic error: hydr	effects 5 GeV/c) omentum: geome calibra ray tra tum e 5%) oogen	try tion	Systematic probable error (%) 1.3 0.6 1.2 1.0 1.0 0.9 0.8 0.5 1.0 3.5% 3.0%		

The cross section for ρ photoproduction from carbon was taken from Pipkin,³³ and that for hydrogen from Blechschmidt *et al.*³⁵

Hence the following corrections to the WAPP yields at the highest invariant mass (489 MeV/ c^2) of the electron pair were obtained: carbon, 0.75%; hydrogen, 0.5%. In view of the uncertainties in this calculation, a correction of $(1.0\pm0.5)\%$ was made to these highest mass points. The corrections to all other points were certainly less than 0.3% and were neglected.

G. Photon Absorption in Target

This effect was calculated using the total pair-production cross section as given by Heitler.³¹ It was also checked experimentally by placing absorbers in the photon beam, to allow for the possibility of electron pairs formed in the target, reaching the quantameter, and giving up their energy. This measurement agreed with the theoretical prediction to within the experimental error. The corrections obtained were for 20 mm of carbon (3.1%) and for 300 mm of hydrogen (1.0%).

H. Positron Annihilation in Spectrometer

Again using cross sections given by Heitler, corrections calculated for this effect varied from 0.4% at $E_{+}=1$ GeV to 0.2% at 2 GeV.

A complete list of corrections and systematic probable errors is given in Table III.

5. RESULTS

A. Single-Arm Electron Rates

As a check on the absolute calibration, solid angle, rate corrections, etc., the single-arm electron rates were calculated theoretically and compared with the experimental data.

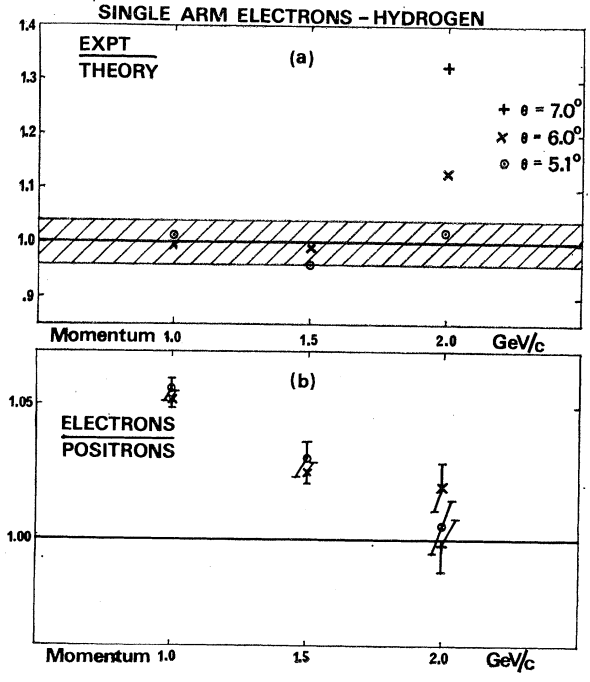


Fig. 12. (a) Average single-arm electron-positron rates: ratio of experiment to theory for the hydrogen target, as a function of momentum and angle. The shaded area represents the over-all systematic normalization error. (b) Ratios of electrons to positrons at the same settings.

²⁵ H. Blechschmidt, J. P. Dowd, B. Elsner, K. Heinloth, K. H. Höhne, S. Raither, J. Rathye, D. Schmidt, J. H. Smith, and J. H. Weber, in *Proceedings of the Third International Symposium on Electron and Photon Interactions at High Energies, Stanford Linear Accelerator Center*, 1967 (Clearing House of Federal Scientific and Technical Information, Washington, D. C., 1968), p. 607.

Two contributions of similar magnitude make up the single-arm electron rates. These are direct electron or positron production at the experimental angle θ , by the Bethe-Heitler process, and production in the forward direction with subsequent scattering by the target nuclei into the spectrometer acceptance. The latter, being proportional to target thickness squared, is referred to as the t^2 effect.

The first contribution was calculated by integrating the BDF formula over all the variables of one arm. The bremsstrahlung spectrum was approximated by the Schiff³⁶ formula. The numerical integration is expected to be accurate to better than 5%. In calculating the second contribution, the cross section for the forward production of electrons was obtained from the sum of the cross sections for production in the fields of (a) the target nuclei and (b) the atomic electrons, as given by Wheeler and Lamb.³⁷ Exchange corrections to the process (b) caused by the identical nature of the two electrons in the final state have been neglected, as have Coulomb corrections to process (a). Both these corrections would decrease the Wheeler-Lamb formulas probably by a few percent.³⁸ The subsequent scattering of the electrons was calculated using the Mott cross section multiplied by the appropriate form factor.

No radiative correction was calculated since it was expected to be considerably less than the systematic

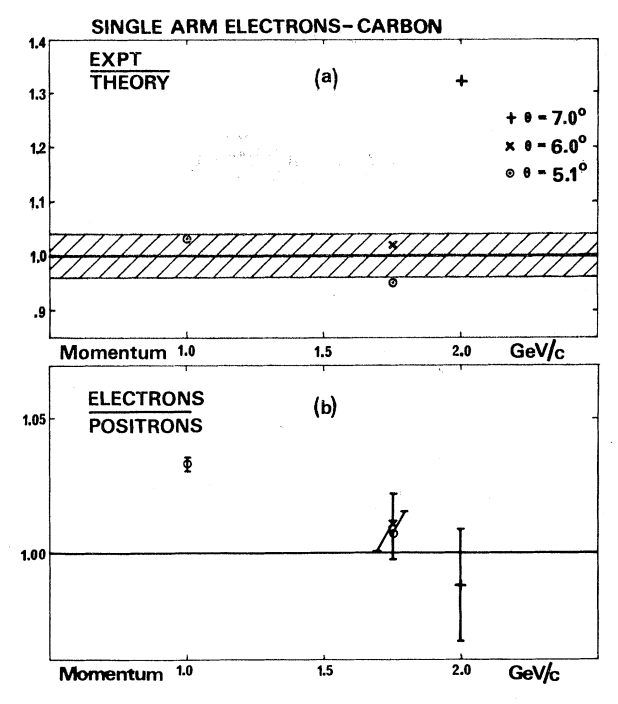


Fig. 13. Results for carbon target (see caption to Fig. 12).

TABLE IV. Results.

Target	Momentum (GeV/c)	Angle (deg)	$Q_m \ ({ m MeV}/c^2)$	Experiment/ theory
Hydrogen Carbon	1.0 1.0 1.5 1.5 2.0 2.0 2.0 1.0 1.75 1.75	5.1 6.0 5.1 6.0 5.1 6.0 7.0 5.1 5.1 6.0	178 209 267 314 356 419 489 178 312 366	0.993±0.050 1.062±0.057 0.953±0.056 1.083±0.046 1.090±0.062 1.055±0.068 1.082±0.073 1.068±0.036 0.972±0.086
	2.0	7.0	489	0.860 ± 0.068

errors involved. However, a bremsstrahlung correction assumed to be half of that for pair production was applied.

Comparison of the average electron-positron rates with the calculated rates is shown for hydrogen in Fig. 12(a) and for carbon in Fig. 13(a). The data plotted on these graphs are the average for the left and right arms, which were always in agreement to within 1%. Statistical errors are too small to show. Agreement between experiment and theory is good in both cases except at the highest values of momentum and production angle, where presumably other processes become dominant, e.g., Dalitz decay of photoproduced π^0 's.

The ratios of electrons to positrons measured at each momentum and angle are plotted against momentum in Figs. 12(b) and 13(b). (Each point is the average value for the electron-positron ratio in the two arms.) These ratios are measured to a very high accuracy since most systematic errors cancel. The significant difference from unity of these ratios may be due to one or more of several causes, e.g., interference between the Bethe-Heitler and Compton processes in the direct production, the exchange corrections mentioned above, etc. However, no single one of these causes is compatible with the observed variation of the effect for the two target materials at fixed momentum and angle. Data taken with the two thicknesses of carbon target indicate that the effect is probably in the t^2 contribution to the yield. Further investigation of this point would be useful, but there is insufficient information at present to identify the cause of this asymmetry.

B. Electron-Pair Rates

The electron-pair production results are shown in Table IV and Fig. 14, in the form of ratios of experimental yields to theoretical predictions, as a function of the invariant mass of the electron pair. The shaded areas in Fig. 14 show the over-all systematic errors (1 standard deviation) from Table II. For both targets the data are consistent with the predictions of QED and with the results of Refs. 5-7.

³⁶ L. I. Schiff, Phys. Rev. **83**, 252 (1951).
³⁷ J. A. Wheeler and W. E. Lamb, Phys. Rev. **55**, 858 (1939).
³⁸ J. Joseph and F. Rohrlich, Rev. Mod. Phys. **30**, 354 (1958).

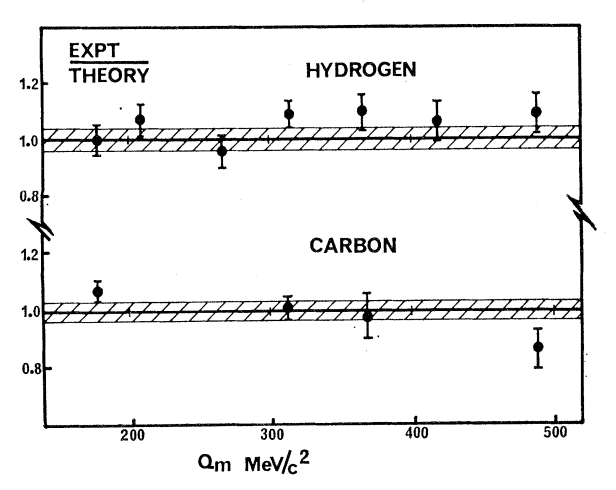


Fig. 14. Wide-angle electron-pair production: ratios of experimental data to QED predictions for hydrogen and carbon targets. Q_m is the invariant mass of the electron pair. The shaded areas represent the over-all systematic normalization errors.

C. Validity of QED

Kroll³⁹ has shown that, to be consistent with general considerations, any deviations from QED in WAPP or WAB must be of at least fourth order in Q_l or Q_m .

By fitting the ratios R, of the experimental data to theoretical predictions, to the formula

$$R = A \pm BQ_{l^4}$$

where A is a systematic normalization constant, the following best fits are obtained:

Hydrogen data:

$$R = (1.024 \pm 0.028) + (5.2 \pm 5.2) (\text{GeV}/c^2)^{-4}O_l^4$$
.

Hydrogen and carbon data:

$$R = (1.042 \pm 0.020) - (4.2 \pm 3.6) (\text{GeV}/c^2)^{-4}Q_l^4$$
.

If B is then interpreted as $B = \Lambda^{-4}$, where Λ is a cutoff parameter, the best fit to all the data yields values

Table V. Values of the cutoff parameter Λ in GeV/c^2 .

		Fit to $R = A + \Lambda^{-4}Qt^4$			
Laboratory	Type of experiment	Most prob- able	confi- dence	Most prob- able	95% confi- dence
DNPL (this expt.)	$\gamma p \rightarrow p e^+ e^- $ $\gamma C \rightarrow C e^+ e^- $	∞	>0.76	0.71	>0.55
DESY ^a Cornell ^b Cornell ^c BNL ^d	$ \gamma C \to Ce^+e^- \gamma C \to C\mu^+\mu^- e^-C \to Ce^-\gamma \mu C \to C\mu\gamma $	1.70 ∞ 1.35 ∞	>1.00 >2.24 >1.11 >0.84	1.29 ∞ 1.10	>1.07 >1.07 >2.02 >0.73

of Λ at the 95% confidence level, as shown in Table V. Also shown here are values of Λ obtained from other significant WAPP and WAB experiments in the same region of the virtual lepton mass. Assuming that electron and muon experiments are equivalent, the world value for the parameter Λ for either sign of deviation from QED is $\Lambda > 1.7$ GeV/ c^2 with 95% confidence.

For the validity of other aspects of QED and electron and muon universality, the reader is referred to the reviews cited in Ref. 12.

ACKNOWLEDGMENTS

The authors greatly appreciate the invaluable assistance of M. D. Rousseau and D. G. Taylor during the early stages of the experiment, and the tireless and enthusiastic support of M. W. Collins and A. E. Groome throughout. They are also indebted to A. J. Egginton and the NINA machine group and M. J. Moore and the technical services group, especially H. Stott. Finally, they would like to acknowledge the encouragement and support of Professor A. W. Merrison and Dr. R. G. P. Voss,

³⁹ N. M. Kroll, Nuovo Cimento 45A, 65 (1966).

<sup>Reference 6.
Reference 10.
Reference 9.
Reference 11.</sup>